

Protection of noisy multipartite entangled states of superconducting qubits via universally robust dynamical decoupling schemes

Akanksha Gautam,^{*} Arvind,[†] and Kavita Dorai[‡]

*Department of Physical Sciences, Indian Institute of Science Education & Research Mohali,
Sector 81 SAS Nagar, Manauli PO 140306 Punjab India.*

We demonstrate the efficacy of the universally robust dynamical decoupling (URDD) sequence to preserve multipartite maximally entangled quantum states on a cloud based quantum computer via the IBM platform. URDD is a technique that can compensate for experimental errors and simultaneously protect the state against environmental noise. To further improve the performance of the URDD sequence, phase randomization (PR) as well as correlated phase randomization (CPR) techniques are added to the basic URDD sequence. The performance of the URDD sequence is quantified by measuring the entanglement in several noisy entangled states (two-qubit triplet state, three-qubit GHZ state, four-qubit GHZ state and four-qubit cluster state) at several time points. Our experimental results demonstrate that the URDD sequence is successfully able to protect noisy multipartite entangled states and its performance is substantially improved by adding the phase randomization and correlated phase randomization sequences.

I. INTRODUCTION

Quantum entanglement is a type of quantum correlation [1, 2] which has wide applications in quantum computing and quantum information processing such as quantum secret sharing [3, 4], quantum cryptography [5], quantum teleportation [6] and quantum dense coding [7]. However, as the number of qubits increases, control of the entire system becomes difficult due to the presence of environmental noise which adversely affects the entanglement present in multipartite systems [8, 9]. Decoherence due to system-environment interaction eventually leads to decay of quantum coherence and is a major hurdle in building actual quantum computers. Various strategies have been proposed to mitigate the effect of decoherence, including quantum error correction [10–12], decoherence free subspace [13, 14] and dynamical decoupling (DD)[15–22]. DD sequences have proved to be successful in protecting the quantum state without requiring any prior knowledge of the environment[23–25].

DD is an open-loop control scheme that involves the application of tailored π pulses on the system that average out the system-environment interactions. Originally the DD sequence was introduced in the case of nuclear magnetic resonance (NMR)[26], from where this sequence evolved to generate complicated sequences to protect the quantum state with high precision such as XY4, concatenated DD (CDD), Knill DD (KDD) and Uhrig DD (UDD) sequences [19, 27–33]. The XY4 sequence was proposed to compensate for the errors accumulated from the repeated application of inverse pulses but it has limited error compensation. The KDD sequence is a robust sequence against pulse errors derived from the composite pulses but requires a higher duty cycle for better effect

[34]. The CDD sequence is constructed from the recursive pulse sequence that eliminates decoherence to an arbitrary order but the number of pulses increases exponentially. Thus, this area of research still needs to be explored to design better DD sequences with limited experimental resources [33]. One such DD sequence called the universally robust dynamical decoupling (URDD) was recently proposed that can compensate higher order pulse errors while the number of pulses increases only linearly and works well for any initial condition [35]. Its superior performance has been verified experimentally in storing coherent optical data in a Pr:YSO crystal. Further, the protection of single-qubit states has been shown experimentally using URDD and other previously known DD sequences on the Rigetti computing platform [36].

A method was proposed to further improve the robustness of DD sequences, called the phase randomization technique, in which a random global phase is added to all π pulses of the DD sequence, with this changing each time the unit of the DD sequence is repeated [37]. Another method called the correlated phase randomization (CPR) technique was proposed which is a variant of the previously proposed phase randomization (PR) technique, wherein the fully random phases are replaced with correlated random phases [38]. These techniques were originally proposed for applications in quantum sensing for correct signal identification in nitrogen-vacancy centers.

Much recent research efforts are focused on increasing the size of quantum systems, which however are more prone to noise and are hence termed noisy intermediate-scale quantum (NISQ) computers. The IBM Quantum Experience is freely providing such a system based on superconducting qubits to the public and several researchers have been successful in implementing real quantum experiments[39–43]. Therefore, implementing protection schemes on this noisy quantum computer is a good test of the efficiency of DD sequences in protecting multipartite entangled states.

^{*} akankshagautam@iisermohali.ac.in

[†] arvind@iisermohali.ac.in

[‡] kavita@iisermohali.ac.in

In this work, we have experimentally demonstrated the preservation of maximally entangled multipartite states (two-qubit triplet state, three-qubit GHZ state and four-qubit GHZ as well as cluster state) generated using superconducting qubits on the cloud-based IBM quantum experience. These maximally entangled quantum states are preserved by the application of URDD sequences on the five-qubit *ibmq_manila* quantum processor. The performance of the URDD sequence is further improved by adding PR as well as CPR sequences. To quantify the performance of URDD sequence and its variant on adding PR and CPR sequences in preserving entangled states, we measured the entanglement witness of each maximally entangled state directly by measuring only a single qubit to verify the preservation of entanglement on protecting the state. Our experimental results show that the URDD sequence is able to successfully preserve the entanglement of multipartite state. The extent to which the state is preserved by URDD sequence is further improved by adding phase and correlated phase randomization techniques.

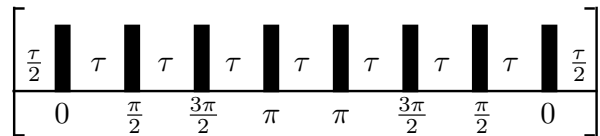
This paper is organized as follows: Sec.II describes the dynamical decoupling sequences used to protect the entangled states. Sec.II A contains details of the URDD sequence and Sec.II B describes the phase randomization technique, while Sec.II C describes the correlated phase randomization technique. Sec.III A contains the experimental details of the implementation of the URDD sequence on the IBM quantum processor and Sec.III B describes the results of directly measuring the entanglement witness of the two-qubit (triplet state), three-qubit (GHZ state) and four-qubit (GHZ and cluster state) maximally entangled states, after applying the DD protection sequences. Sec.IV presents some concluding remarks.

II. UNIVERSALLY ROBUST DYNAMICAL DECOUPLING

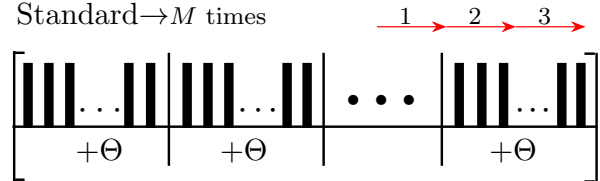
Dynamical decoupling (DD) is a technique that consists of sequences of periodic π pulses applied on the quantum system, where each π pulse is separated by free evolution delays of time τ . The phases of π pulses and delays play an important role in the performance of DD sequence where appropriate choice of phases can make the DD sequence robust against the pulse errors. It is well known that pulse imperfections are a major factor that limit the performance of DD sequences. To compensate these pulse errors, the universally robust DD (URDD) sequence has been recently designed which shows a superior performance.

The URDD sequence is designed for an even number of pulses where the propagator of the n -pulse DD sequence is written as: $U^n = U(\phi_n) \dots U(\phi_2)U(\phi_1)$ where the phases ϕ_1, \dots, ϕ_n are the free control parameters that need to be appropriately designed and each pulse completely inverts the population i.e. transition probability $p = 1$ in the ideal case [35]. Thus, the target propaga-

(a) UR8DD Sequence



(b) Standard $\rightarrow M$ times



(c) PR and CPR $\rightarrow M$ times

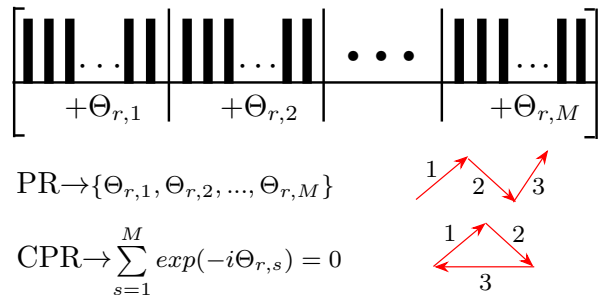


FIG. 1. (a) A basic unit of a universally robust DD sequence of order 8 (UR8DD) where the filled black rectangles represent π pulses. The phase of each pulse is written below each rectangle and τ denotes the delay between pulses. (b) The standard DD protocol where each UR8DD unit is repeated M times, with a common global phase Θ added to each unit of the UR8DD sequence (example is shown in red). (c) The randomization protocol (PR), with a random global phase $\Theta_{r,s}$ being added to each unit of the UR8DD sequence; in the correlated randomization protocol (CPR), a constraint is imposed on the random phase (examples of PR and CPR are shown in red).

tor is defined as $U_0 = U^{(n)}(p = 1) = (-1)^{n/2} \exp(i\beta \hat{I}_z)$ where $\beta = 2 \sum_{k=1}^{n/2} (\phi_{2k} - \phi_{2k-1})$. The performance of the DD sequence is measured by fidelity:

$$F = \frac{1}{2} |Tr(U_0^\dagger U^{(n)})| = 1 - \delta_n \quad (1)$$

where U_0 is the target operator and $U^{(n)}$ is the operator of the DD sequence that depends on relative phases between pulses ϕ_k (phase of the k th pulse) and δ_n denotes the infidelity of n -pulse DD sequence. The goal is to derive the control phases ϕ_k which can minimize the infidelity of the DD sequence and for that the Taylor expansion is taken with respect to errors in the control parameters by finding appropriate phases. The phases of the n -pulse URDD sequence is given in the general form as [35]:

$$\phi_k^{(n)} = \frac{(k-1)(k-2)}{2} \Phi^{(n)} + (k-1)\phi_2, \quad (2)$$

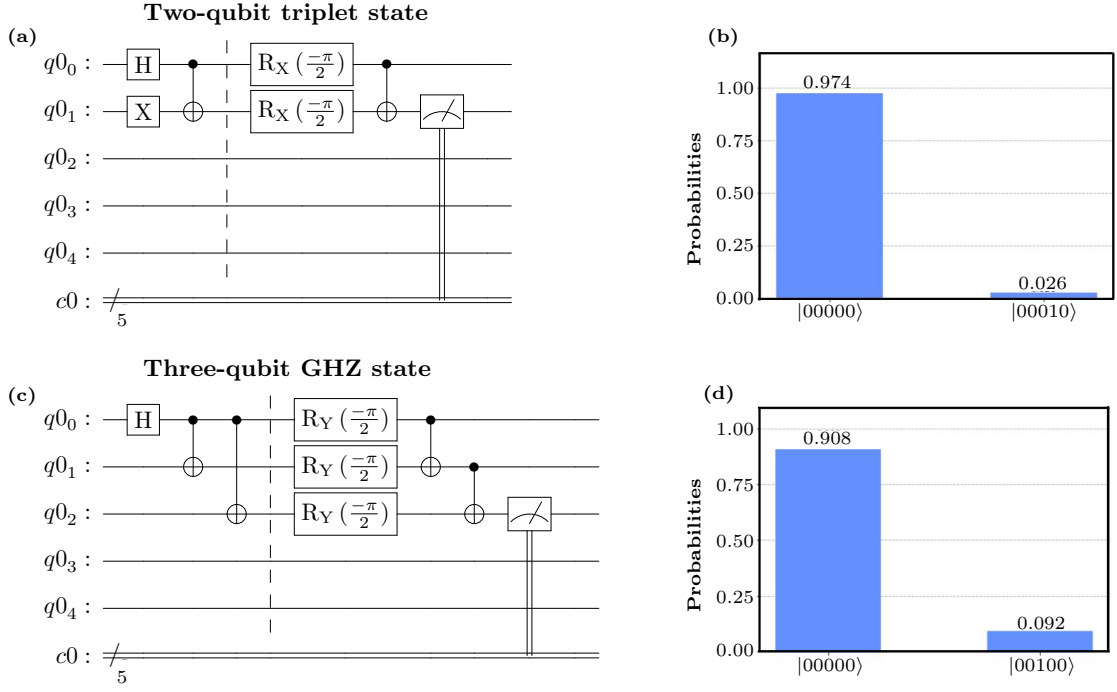


FIG. 2. IBM quantum circuit to create an entangled state. (a) The first block of the circuit creates a two-qubit triplet state while the second block applies the quantum map $O_2 = \text{CNOT}_{23} \cdot \bar{X}_2 \cdot \bar{X}_1$ to measure the expectation value of $\langle \sigma_{1y} \sigma_{2y} \rangle$ by detecting the second qubit in the $|0\rangle$ and the $|1\rangle$ state with the values $p_0 = 0.974$ and $p_1 = 0.026$, respectively. (b) Histogram representing probabilities of obtaining the second qubit in the $|0\rangle$ and the $|1\rangle$ state with the values $p_0 = 0.974$ and $p_1 = 0.026$, respectively. (c) The first block of the circuit creates a three-qubit GHZ state and while the second block applies the quantum map $P_4 = \text{CNOT}_{23} \cdot \bar{Y}_3 \cdot \text{CNOT}_{12} \cdot \bar{Y}_2 \cdot \bar{Y}_1$ to measure the expectation value of $\langle \sigma_{1x} \sigma_{2x} \sigma_{3x} \rangle$ by detecting the third qubit in the $|0\rangle$ and the $|1\rangle$ state with the values $p_0 = 0.908$ and $p_1 = 0.092$, respectively. (d) Histogram representing probabilities of obtaining the third qubit in the $|0\rangle$ and the $|1\rangle$ state with the values $p_0 = 0.908$ and $p_1 = 0.092$, respectively.

where

$$\Phi^{(4m)} = \pm \frac{\pi}{m}, \quad \Phi^{(4m+2)} = \pm \frac{2m\pi}{2m+1} \quad (3)$$

k is the phase of k th pulse of the n -pulse URDD sequence and ϕ_2 is arbitrarily chosen.

A. Standard DD Method

In the standard method, the DD sequence is repetitively applied as shown in Fig.1(b) where each unit of the DD sequence corresponds to an identity operation in the ideal condition; however practically such operations are not possible due to the presence of experimental errors. Thus, each unit of the DD sequence is written as [37]:

$$U_{unit} = \begin{bmatrix} 1 & iC\epsilon \\ iC^*\epsilon & 1 \end{bmatrix} + O(\epsilon^2) \quad (4)$$

where C is a complex number that depends on the structure of the DD sequence and ϵ is the experimental error. When each DD unit is repeated M times as $U_M = U_{unit} \dots U_{unit} = (U_{unit})^M$, the errors present in one unit get accumulated, and the matrix form of the DD

sequence becomes [37]:

$$U_M = \begin{bmatrix} 1 & iMC\epsilon \\ iMC^*\epsilon & 1 \end{bmatrix} + O(\epsilon^2) \quad (5)$$

where the off-diagonal terms of the matrix show that the errors get accumulated linearly upon several applications of the DD sequence.

B. Phase Randomization Method

As explained in Sec.II A, errors get accumulated upon applying the basic unit of DD sequence M times. In the phase randomization (PR) technique [37], a random global phase $\Theta_{r,s}$ (r denotes random phase and s denotes s th unit of DD sequence) is introduced to all π pulses of s th unit of DD sequence and the random phase changes each time the unit of DD sequence is repeated (Fig.1(c)). The matrix form of the DD sequence after adding the PR sequence is given by [37]:

$$U_M = U_{unit}(\Theta_{r,M}) \dots U_{unit}(\Theta_{r,2}) U_{unit}(\Theta_{r,1}) \quad (6)$$

$$= \begin{bmatrix} 1 & iZ_{r,M} MC\epsilon \\ iZ_{r,M}^* MC^*\epsilon & 1 \end{bmatrix} + O(\epsilon^2) \quad (7)$$

where $Z_{r,M} = 1/M \sum_{s=1}^M \exp(-i\Theta_{r,s})$. The contribution of $Z_{r,M}$ in the off-diagonal terms of the matrix serves to improve the robustness of the overall DD sequence and the factor $Z_{r,M}$ act as a random walk due to the random phase $\Theta_{r,s}$.

C. Correlated Phase Randomization Method

In the correlated phase randomization (CPR) technique [38], a condition is imposed in the PR technique where the random phases should be chosen such that $Z_{r,M} = 1/M \sum_{s=1}^M \exp(-i\Theta_{r,s}) = 0$. This condition erases the off-diagonal terms of the matrix given in Eq.7 and thus suppresses the experimental errors more effectively as compared to PR technique. The CPR technique is also efficient because it does not depend on the value of M , and even smaller number of M s are sufficient to erase the error, whereas the phase randomization technique requires a larger number of M s to suppress the error.

III. EXPERIMENTAL DEMONSTRATION OF PROTECTION OF MAXIMALLY ENTANGLED MULTIPARTITE STATE ON THE IBM QUANTUM PROCESSOR

A. Experimental details

The IBM quantum processor is a freely available online service that gives access to superconducting transmon based qubits [44]. We used the five-qubit *ibmq_manila* quantum processor, chosen as the average T_1 rate is greater than T_2 with phase damping being a dominant noise channel. T_1 values for the qubits were between 126–151 μ s and T_2 values were between 50–66 μ s. Length of single qubit gate of *ibmq_manila* quantum processor was 35.5ns while error of single qubit gate was of the order 10^{-3} and readout errors were of the order 10^{-2} . Using four qubits of the quantum processor, we demonstrate the protection of two-qubit (triplet), three-qubit (GHZ-state) and four-qubit (GHZ and cluster states) multipartite entangled states. The quantum circuit to create an entangled state on the IBM processor are shown in Fig.2(a,c) and Fig.4(a,c) where each circuit was implemented 8192 times to compute the Born probabilities.

We protect the entangled states using a URDD sequence of order 8, which we term the UR8DD sequence. Mathematically, the total operator of one unit of the UR8DD sequence is written as UR8DD = $F(\tau/2)U(\phi_8)F(\tau)...F(\tau)U(\phi_1)F(\tau/2)$ where F corresponds to free evolution operation for time period τ and $U(\phi_k)$ denotes the k th π pulse operation about the axis ϕ_k . The sequence of phases of π pulses of UR8DD sequence are $\phi_k = (0, \pi/2, 3\pi/2, \pi, \pi, 3\pi/2, \pi/2, 0)$. On the IBM quantum processor, the UR8DD pulses are applied

using single-qubit quantum gates and an arbitrary single-qubit gate can be applied as

$$G(\alpha, \beta, \gamma) = \begin{bmatrix} \cos(\alpha/2) & -e^{i\gamma} \sin(\alpha/2) \\ e^{i\beta} \sin(\alpha/2) & e^{i(\beta+\gamma)} \cos(\alpha/2) \end{bmatrix} \quad (8)$$

where k th π pulse used in UR8DD sequence can be implemented as a single-qubit quantum gate by specifying the parameters as $U(\phi_k) = G(\pi, \phi_k - \pi/2, \pi/2 - \phi_k)$. For the free evolution between the pulses and to track the free evolution dynamics of entangled states, identity gates are used. The total time period (T) for which one unit of UR8DD sequence applied was 0.84 μ s where free evolution delay time between two pulses was 70ns and total number of gates involved in one unit was 24. To protect multipartite entangled states, UR8DD sequences were implemented simultaneously on each qubit contributing in generating entanglement of the state. One unit of the UR8DD sequence was applied several times (maximum 9 times) to preserve the entanglement for a longer time.

Further to improve the performance of the phase randomization technique, we repeated the experiments by adding random phases to all π pulses of each unit of UR8DD where the k th pulse of UR8DD sequence was applied along the axis $\phi_k + \Theta_{r,m}$. The experiments were repeated a maximum of 9 times ($M = 9$) after adding phase randomization technique to UR8DD sequence. Phase randomization technique can be improved further by using correlated phase randomization technique where fully random phases are replaced with correlated phases. This technique suppresses the experimental errors more efficiently as compared to PR technique and works well even for less number of repetition of UR8DD sequence. Thus, we repeated the experiment by adding correlated phase to UR8DD sequence that require minimum two times repetition of UR8DD sequence. In each experiment, total number of correlated phases are divided into combinations of two sets of phases and three sets of phases such that the condition $Z_{r,M} = 1/M \sum_{s=1}^M \exp(-i\Theta_{r,s}) = 0$ is satisfied. For example, if the UR8DD sequence is applied for 5 times, then in the first two units of the UR8DD sequence, phases should be such that $Z_{r,2} = \exp[-i(\Theta_{r,1} + \Theta_{r,2})]/2 = 0$ and similarly, in the next three units of the UR8DD sequence, $Z_{r,3} = \exp[-i(\Theta_{r,3} + \Theta_{r,4} + \Theta_{r,5})]/3 = 0$. Thus the overall condition of CPR technique is satisfied.

B. Entanglement Witness

An entanglement witness (W) can detect the presence of entanglement in a quantum state by directly measuring the observables [45–50]. A quantum state ρ is an entangled state if there exists a Hermitian operator (called entanglement witness) such that $Tr[W\rho] < 0$ and if $Tr[W\rho] \geq 0$ then the quantum state is separable. Therefore, the negative expectation of the witness operator W signifies the presence of entanglement.

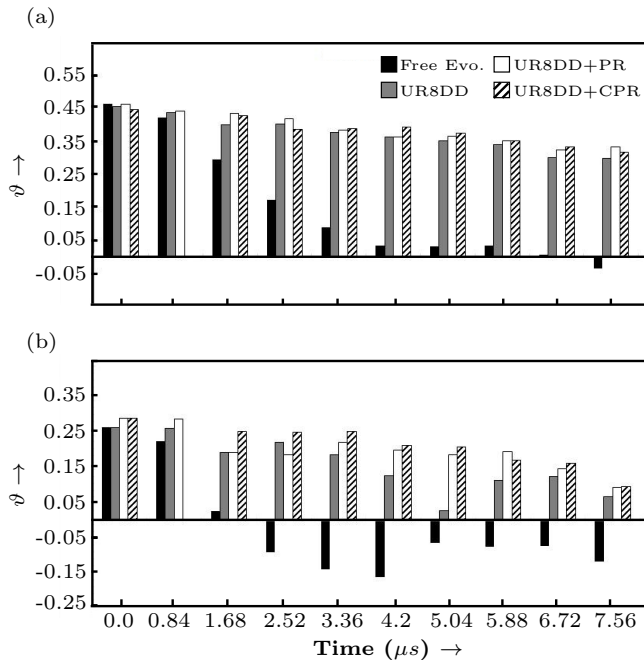


FIG. 3. Bar plots of the entanglement parameter (ϑ) versus time (μs) of: (a) the two-qubit triplet state and (b) the three-qubit GHZ state. The black solid bars represent ϑ of the states without applying any DD protection, the grey solid bars represent ϑ of the states after applying the UR8DD sequence, the white bars represent ϑ of the states after applying the UR8DD sequence and adding the PR sequence (UR8DD+PR), and the black cross-hatched bars represent ϑ of the states after applying the UR8DD sequence and adding CPR sequence (UR8DD+CPR).

The presence of entanglement in quantum states at different time points are measured by entanglement witness during free evolution and while implementing the UR8DD sequence and after adding phase and correlated randomization methods. We measured the entanglement witness and plotted the bar graph of entanglement parameter by taking negative of entanglement witness ($\vartheta = -\text{Tr}[W\rho]$).

Thus, we experimentally measured the entanglement parameter of the two-qubit triplet state, the three-qubit GHZ state and the four-qubit GHZ state and cluster states at different time points, to quantify the preservation of entanglement in these states.

Two-qubit triplet state: We experimentally created the two-qubit entangled state (triplet state) using two qubits of five qubits *ibmq_manila* quantum processor. The quantum circuit to create the state is shown in first block of Fig.2(a). We first studied the dynamics of entanglement present in triplet state (ρ_{TS}) under free evolution and then we protected the entanglement by implementing UR8DD sequence on both qubits simultaneously. Further, we added phase randomization and correlated phase randomization techniques to UR8DD sequence to enhance its performance in extending the time

period for which state can be protected. After each run of DD sequence, the presence of entanglement is detected by measuring entanglement witness directly where one run of DD sequence is of $0.84 \mu s$. Entanglement witness operator (W_{TS}^2) for triplet state can be written in linear combination of $\sigma_{1x}\sigma_{2x}$, $\sigma_{1y}\sigma_{2y}$ and $\sigma_{1z}\sigma_{2z}$ Pauli operator as [46]

$$W_{TS}^2 = \frac{1}{4}(I_2 - \sigma_{1x}\sigma_{2x} - \sigma_{1y}\sigma_{2y} + \sigma_{1z}\sigma_{2z}) \quad (9)$$

where $\{\sigma_x, \sigma_y, \sigma_z\}$ are single qubit Pauli basis. Experimentally, we measured witness operator W_{TS}^2 by measuring expectation value of three Pauli operators where expectation of each Pauli operator was found experimentally by mapping the state ρ to ρ_j through unitary operator as $\rho_j = O_j\rho O_j^\dagger$ which is followed by observing $\langle\sigma_{2z}\rangle$ for the state ρ_j . Quantum circuit for one of the mapping is shown in second block of Fig.2(a) and the details of mapping of Pauli operators to the single qubit σ_z Pauli operator are given in Table I where $Y_a = R_Y(\frac{\pi}{2})$, $\bar{X}_a = R_X(\frac{-\pi}{2})$ and a denotes the qubit number.

TABLE I. Observables required to measure the entanglement witness for two qubits (triplet state) are mapped to Pauli σ_z operators through the initial state transformation $\rho \rightarrow \rho_j = O_j\rho O_j^\dagger$.

Observable expectations	Unitary operator
$\langle\sigma_{1x}\sigma_{2x}\rangle = \text{Tr}[\rho_1 \cdot \sigma_{2z}]$	$O_1 = \text{CNOT} \cdot Y_2 \cdot Y_1$
$\langle\sigma_{1y}\sigma_{2y}\rangle = \text{Tr}[\rho_2 \cdot \sigma_{2z}]$	$O_2 = \text{CNOT} \cdot \bar{X}_2 \cdot \bar{X}_1$
$\langle\sigma_{1y}\sigma_{2y}\rangle = \text{Tr}[\rho_3 \cdot \sigma_{2z}]$	$O_3 = \text{CNOT}$

Theoretically, the value of entanglement parameter $\vartheta = -\text{Tr}[W_{TS}^2 \cdot \rho_{TS}]$ for two-qubit triplet state is 0.5 and the quantum state remains entangled until $\vartheta > 0$. Experimentally, we found the entanglement parameter of triplet state on IBM quantum processor as $\vartheta_{exp} = 0.461$. We plotted the bar graph of entanglement parameter ϑ found experimentally at different time points corresponding to each DD sequences (UR8DD, UR8DD+PR and UR8DD+CPR) and free evolution. The result is shown in Fig.3(a), from where it can be seen that UR8DD sequence has protected the entanglement very well and its performance is improved further on adding random phase and correlated random phase to it. Without protection, entanglement dies at $7.56 \mu s$ and protection with UR8DD sequence, 80% of entanglement is preserved, with UR8DD+PR sequence, 72.1% of entanglement is preserved whereas with UR8DD+CPR sequence, 71.1% of entanglement is preserved.

Three-qubit GHZ state: We experimentally constructed three-qubit GHZ state (ρ_{GHZ}^3) using three qubits of five qubits *ibmq_manila* quantum processor through the quantum circuit shown in first block of Fig.2(c). We first studied the dynamics of entanglement present in three-qubit GHZ state under free evolution. Then we protected the quantum state by applying

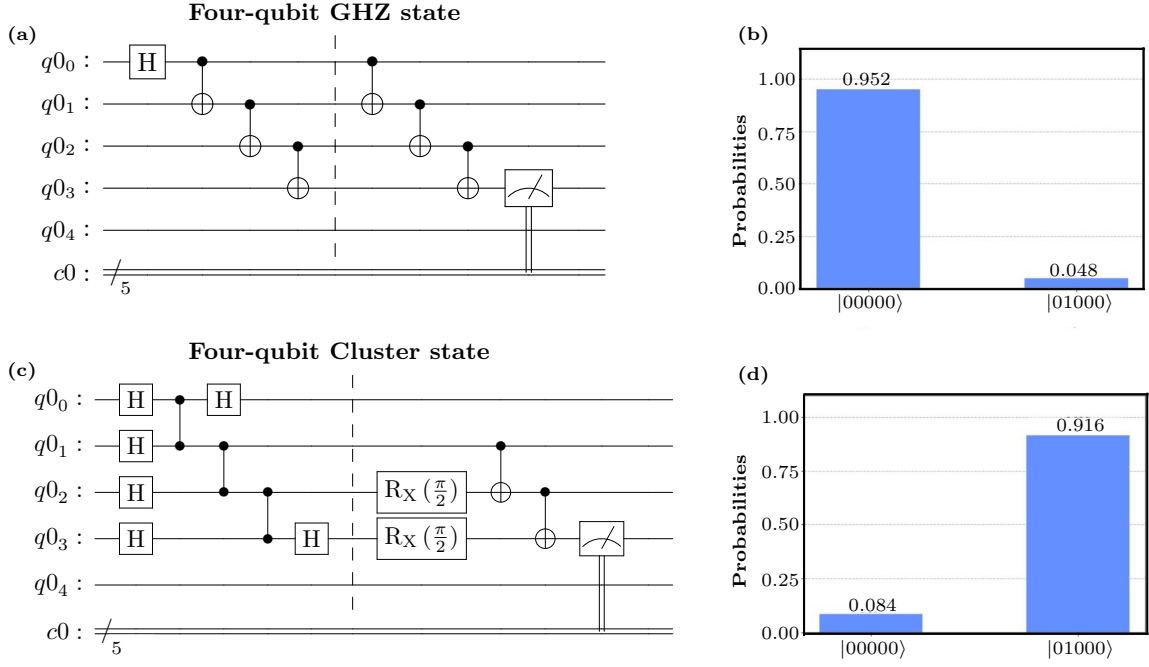


FIG. 4. The IBM quantum circuit to create four-qubit entangled states. (a) The first block of the quantum circuit creates a four-qubit GHZ state and the second block applies the quantum map $Q_7 = \text{CNOT}_{34} \cdot \text{CNOT}_{23} \cdot \text{CNOT}_{12}$ to measure the expectation value of $\langle \sigma_{1z} \sigma_{2z} \sigma_{3z} \sigma_{4z} \rangle$ by detecting the fourth qubit in the z basis. (b) Histogram representing probabilities of obtaining the fourth qubit in the $|0\rangle$ and the $|1\rangle$ state with the values $p_0 = 0.952$ and $p_1 = 0.048$, respectively. (c) The first block of the circuit creates a four-qubit cluster state and the second block applies the quantum map $Q_{20} = \text{CNOT}_{34} \cdot X_4 \cdot \text{CNOT}_{23} \cdot X_3$ to measure the expectation value of $\langle \sigma_{2z} \sigma_{3y} \sigma_{4y} \rangle$ by detecting the fourth qubit in the z basis where $X_3 = X_4 = R_X(\frac{\pi}{2})$. (d) Histogram representing probabilities of obtaining the fourth qubit in the $|0\rangle$ and the $|1\rangle$ state with the values $p_0 = 0.084$ and $p_1 = 0.916$, respectively.

UR8DD sequence simultaneously on three qubits and its performance is improved by adding random phase and correlated random phase technique.

TABLE II. Observables required to measure the entanglement witness for three qubits (GHZ state) are mapped to Pauli σ_z operators through the initial state transformation $\rho \rightarrow \rho_j = P_j \rho P_j^\dagger$.

Observable expectations	Unitary operator
$\langle \sigma_{2z} \sigma_{3z} \rangle = \text{Tr}[\rho_1 \cdot \sigma_{3z}]$	$P_1 = \text{CNOT}_{23}$
$\langle \sigma_{1z} \sigma_{3y} \rangle = \text{Tr}[\rho_2 \cdot \sigma_{3z}]$	$P_2 = \text{CNOT}_{13}$
$\langle \sigma_{1z} \sigma_{2z} \rangle = \text{Tr}[\rho_3 \cdot \sigma_{2z}]$	$P_3 = \text{CNOT}_{12}$
$\langle \sigma_{1x} \sigma_{2x} \sigma_{3x} \rangle = \text{Tr}[\rho_4 \cdot \sigma_{3z}]$	$P_4 = \text{CNOT}_{23} \cdot \bar{Y}_3 \cdot \text{CNOT}_{12} \cdot \bar{Y}_2 \cdot \bar{Y}_1$
$\langle \sigma_{1x} \sigma_{2y} \sigma_{3y} \rangle = \text{Tr}[\rho_5 \cdot \sigma_{3z}]$	$P_5 = \text{CNOT}_{23} \cdot X_3 \cdot \text{CNOT}_{12} \cdot X_2 \cdot \bar{Y}_1$
$\langle \sigma_{1y} \sigma_{2x} \sigma_{3y} \rangle = \text{Tr}[\rho_6 \cdot \sigma_{3z}]$	$P_6 = \text{CNOT}_{23} \cdot X_3 \cdot \text{CNOT}_{12} \cdot \bar{Y}_2 \cdot X_1$
$\langle \sigma_{1y} \sigma_{2x} \sigma_{3y} \rangle = \text{Tr}[\rho_7 \cdot \sigma_{3z}]$	$P_7 = \text{CNOT}_{23} \cdot \bar{Y}_3 \cdot \text{CNOT}_{12} \cdot X_2 \cdot X_1$

To measure how well entanglement is protected, entanglement witness is measured experimentally at different time points without applying DD sequence and after applying DD sequence. Entanglement witness operator for three qubit GHZ state can be written in linear combina-

tion of seven Pauli operators as [46, 51]

$$W_{GHZ}^3 = \frac{1}{8} (3I_3 - \sigma_{2z} \sigma_{3z} - \sigma_{1z} \sigma_{3z} - \sigma_{1z} \sigma_{2z} - \sigma_{1x} \sigma_{2x} \sigma_{3x} + \sigma_{1x} \sigma_{2y} \sigma_{3y} + \sigma_{1y} \sigma_{2x} \sigma_{3y} + \sigma_{1y} \sigma_{2y} \sigma_{3x}) \quad (10)$$

Experimentally, expectation value of each Pauli operators was measured to compute entanglement witness by mapping the state ρ to ρ_j through unitary operator as $\rho_j = P_j \rho P_j^\dagger$ which was followed by observing single qubit $\langle \sigma_{2z} \rangle$ or $\langle \sigma_{3z} \rangle$ for the ρ_j . Quantum circuit for one of the mapping of three qubit is shown in second block of Fig.2(c) and the details of all Pauli operators required to be measured for computing entanglement witness are given in Table II where $X_b = R_X(\frac{\pi}{2})$, $\bar{Y}_b = R_Y(\frac{-\pi}{2})$ and b denotes the qubit number. Theoretically, entanglement parameter is computed for three-qubit GHZ state using entanglement witness as $\vartheta = -\text{Tr}[W_{GHZ}^3 \rho_{GHZ}^3]$ and its value is $\vartheta = 0.5$ while GHZ state remains entangled until $\vartheta > 0$. Experimentally, we got the entanglement parameter of initial three-qubit GHZ state constructed on IBM quantum processor as $\vartheta_{exp} = 0.298$. We plotted the entanglement parameter ϑ versus time corresponding to each DD sequence and free evolution as shown in Fig.3(b). Our results show that three-qubit GHZ state

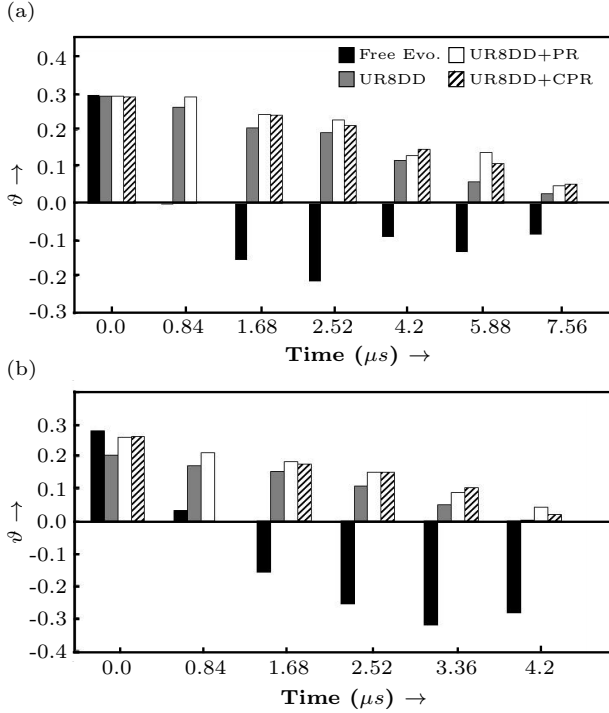


FIG. 5. Bar plots of the entanglement parameter (ϑ) versus time (μs) of: (a) the four-qubit GHZ state and (b) the four-qubit cluster state. The black solid bars represent ϑ of both states without applying any DD protection, the grey solid bars represent ϑ of both states after applying the UR8DD sequence, the white bars represent ϑ of both states after applying the UR8DD sequence and adding a PR sequence (UR8DD+PR) and the black cross-hatched bars represent ϑ of both states after applying the UR8DD sequence and adding a CPR sequence (UR8DD+CPR).

is very fragile as it can be seen that entanglement parameter (ϑ) decays very fast under free evolution of superconducting qubits and entanglement is protected very well on applying UR8DD sequence and its performance is improved on adding PR and CPR technique. Without protection, entanglement dies at $2.52\mu\text{s}$ and on protecting state with UR8DD sequence, 84.4% of entanglement is preserved, with UR8DD+PR sequence, 70.6% of entanglement is preserved whereas with UR8DD+CPR sequence, 94.8% of entanglement is preserved.

Four-qubit GHZ and cluster state: We next experimentally constructed four-qubit maximally entangled state, GHZ (ρ_{GHZ}^4) and Cluster state (ρ_{CS}^4) using four qubits of *ibmq-manila* quantum processor and quantum circuits to create GHZ and Cluster state are shown in Fig.4(a) and Fig.4(c) respectively. We studied the dynamics of free evolution of entanglement present in both four-qubit GHZ and Cluster state. We then protected both state by implementing UR8DD sequence and its variants on four qubits simultaneously. To observe how well entanglement is preserved in both states, entanglement witness was measured at different time points without applying DD sequence and after applying DD

sequence. Entanglement witness operator for four-qubit GHZ state (W_{GHZ}^4) and Cluster state (W_{CS}^4) can be written as [49, 50, 52]

$$W_{GHZ}^4 = \frac{1}{16}(7I_4 - E_1 - E_2 - E_3 - E_4 - E_5 - E_6 - E_7 - E_8 - E_9 + E_{10} + E_{11} + E_{12} + E_{13} + E_{14} + E_{15}) \quad (11)$$

$$W_{CS}^4 = \frac{1}{16}(7I_4 - E_1 - E_6 - E_7 - E_{11} - E_{12} - E_{13} - E_{14} - E_{16} - E_{17} + E_{18} + E_{19} + E_{20} + E_{21} + E_{22} + E_{23}) \quad (12)$$

where E_x 's are Pauli operator

$$\begin{aligned} E_1 &= \sigma_{3z}\sigma_{4z}, & E_9 &= \sigma_{1y}\sigma_{2y}\sigma_{3y}\sigma_{4y}, & E_{17} &= \sigma_{1z}\sigma_{3x}\sigma_{4x} \\ E_2 &= \sigma_{2z}\sigma_{4z}, & E_{10} &= \sigma_{1x}\sigma_{2x}\sigma_{3y}\sigma_{4y}, & E_{18} &= \sigma_{1x}\sigma_{2x}\sigma_{4x} \\ E_3 &= \sigma_{2z}\sigma_{3z}, & E_{11} &= \sigma_{1x}\sigma_{2y}\sigma_{3x}\sigma_{4y}, & E_{19} &= \sigma_{1x}\sigma_{2x}\sigma_{3z} \\ E_4 &= \sigma_{1z}\sigma_{4z}, & E_{12} &= \sigma_{1x}\sigma_{2y}\sigma_{3y}\sigma_{4x}, & E_{20} &= \sigma_{2z}\sigma_{3y}\sigma_{4y}, \\ E_5 &= \sigma_{1z}\sigma_{3z}, & E_{13} &= \sigma_{1y}\sigma_{2x}\sigma_{3x}\sigma_{4y}, & E_{21} &= \sigma_{1z}\sigma_{3y}\sigma_{4y}, \\ E_6 &= \sigma_{1z}\sigma_{2z}, & E_{14} &= \sigma_{1y}\sigma_{2x}\sigma_{3y}\sigma_{4x}, & E_{22} &= \sigma_{1y}\sigma_{2y}\sigma_{4z}, \\ E_7 &= \sigma_{1z}\sigma_{2z}\sigma_{3z}\sigma_{4z}, & E_{15} &= \sigma_{1y}\sigma_{2y}\sigma_{3x}\sigma_{4x}, \\ E_8 &= \sigma_{1x}\sigma_{2x}\sigma_{3x}\sigma_{4x}, & E_{16} &= \sigma_{2z}\sigma_{3x}\sigma_{4x}, \\ E_{23} &= \sigma_{1y}\sigma_{2y}\sigma_{3z} \end{aligned}$$

Experimentally, expectation value of each Pauli operator was measured to compute entanglement witness of both state by mapping the state from ρ to ρ_j through unitary operator as $\rho_j = Q_j\rho Q_j^\dagger$ which was followed by observing single qubit ($\langle\sigma_{3z}\rangle$ or $\langle\sigma_{4z}\rangle$) for ρ_j . Quantum circuit for one of the mapping of each four qubit GHZ state and Cluster state are shown in second block of Fig.4(a) and Fig.4(b) respectively and details of all Pauli operators are given in Table.III. Entanglement witness is used to compute entanglement parameter for both states and theoretically, which is found as $\vartheta = -\text{Tr}[W_{GHZ}^4\rho_{GHZ}^4] = 0.5$ for GHZ state and $\vartheta = -\text{Tr}[W_{CS}^4\rho_{CS}^4] = 0.5$ for Cluster State. Absence of entanglement is determined when entanglement parameter is $\vartheta \leq 0$. Experimentally, entanglement parameter was computed for initial four-qubit GHZ and Cluster state as $\vartheta_{exp} = 0.296$ and $\vartheta_{exp} = 0.282$ respectively.

We plotted the bar graph of the entanglement parameter versus time for the GHZ state and the cluster state corresponding to each DD sequence (UR8DD, UR8DD+PR, UR8DD+CPR) and for free evolution without protection (shown in Fig.5(a) and Fig.5(b)). From the bar graph, we observe that the four-qubit GHZ and cluster states are very fragile as compared to the two-qubit triplet state and the three-qubit GHZ state and hence the entanglement parameter of these states decays very quickly. On applying the UR8DD sequence, the entanglement is protected very well and the preservation is improved upon applying variants of the UR8DD sequence, namely, the PR and CPR techniques. For the four-qubit GHZ state, the entanglement dies at $1.68\mu\text{s}$ and on protecting the state with UR8DD

TABLE III. Observables required to measure the entanglement witness for four qubits (GHZ and cluster states) are mapped to Pauli z operators through the initial state transformation $\rho \rightarrow \rho_j = Q_j \rho Q_j^\dagger$.

Observable	Unitary operator	Observable	Unitary operator
$E_1 = \text{Tr}[\rho_1 \cdot \sigma_{4z}]$	$Q_1 = \text{CNOT}_{34}$	$E_{13} = \text{Tr}[\rho_{13} \cdot \sigma_{4z}]$	$Q_{13} = \text{CNOT}_{34} \cdot X_4 \cdot \text{CNOT}_{23} \cdot \bar{Y}_3 \cdot \text{CNOT}_{12} \cdot \bar{Y}_2 \cdot X_1$
$E_2 = \text{Tr}[\rho_2 \cdot \sigma_{4z}]$	$Q_2 = \text{CNOT}_{13}$	$E_{14} = \text{Tr}[\rho_{14} \cdot \sigma_{4z}]$	$Q_{14} = \text{CNOT}_{34} \cdot \bar{Y}_4 \cdot \text{CNOT}_{23} \cdot X_3 \cdot \text{CNOT}_{12} \cdot \bar{Y}_2 \cdot X_1$
$E_3 = \text{Tr}[\rho_3 \cdot \sigma_{3z}]$	$Q_3 = \text{CNOT}_{23}$	$E_{15} = \text{Tr}[\rho_{15} \cdot \sigma_{4z}]$	$Q_{15} = \text{CNOT}_{34} \cdot \bar{Y}_4 \cdot \text{CNOT}_{23} \cdot \bar{Y}_3 \cdot \text{CNOT}_{12} \cdot X_2 \cdot X_1$
$E_4 = \text{Tr}[\rho_4 \cdot \sigma_{4z}]$	$Q_4 = \text{CNOT}_{14}$	$E_{16} = \text{Tr}[\rho_{16} \cdot \sigma_{4z}]$	$Q_{16} = \text{CNOT}_{34} \cdot \bar{Y}_4 \cdot \text{CNOT}_{23} \cdot \bar{Y}_3$
$E_5 = \text{Tr}[\rho_5 \cdot \sigma_{3z}]$	$Q_5 = \text{CNOT}_{13}$	$E_{17} = \text{Tr}[\rho_{17} \cdot \sigma_{4z}]$	$Q_{17} = \text{CNOT}_{34} \cdot \bar{Y}_4 \cdot \text{CNOT}_{13} \cdot \bar{Y}_3$
$E_6 = \text{Tr}[\rho_6 \cdot \sigma_{2z}]$	$Q_6 = \text{CNOT}_{12}$	$E_{18} = \text{Tr}[\rho_{18} \cdot \sigma_{3z}]$	$Q_{18} = \text{CNOT}_{23} \cdot \text{CNOT}_{12} \cdot \bar{Y}_2 \cdot \bar{Y}_1$
$E_7 = \text{Tr}[\rho_7 \cdot \sigma_{4z}]$	$Q_7 = \text{CNOT}_{34} \cdot \text{CNOT}_{23} \cdot \text{CNOT}_{12}$	$E_{19} = \text{Tr}[\rho_{19} \cdot \sigma_{4z}]$	$Q_{19} = \text{CNOT}_{23} \cdot \text{CNOT}_{12} \cdot \bar{Y}_2 \cdot \bar{Y}_1$
$E_8 = \text{Tr}[\rho_8 \cdot \sigma_{4z}]$	$Q_8 = \text{CNOT}_{34} \cdot \bar{Y}_4 \cdot \text{CNOT}_{23} \cdot \bar{Y}_3 \cdot \text{CNOT}_{12} \cdot \bar{Y}_2 \cdot \bar{Y}_1$	$E_{20} = \text{Tr}[\rho_{20} \cdot \sigma_{4z}]$	$Q_{20} = \text{CNOT}_{34} \cdot X_4 \cdot \text{CNOT}_{23} \cdot X_3$
$E_9 = \text{Tr}[\rho_9 \cdot \sigma_{4z}]$	$Q_9 = \text{CNOT}_{34} \cdot X_4 \cdot \text{CNOT}_{23} \cdot X_3 \cdot \text{CNOT}_{12} \cdot X_2 \cdot X_1$	$E_{21} = \text{Tr}[\rho_{21} \cdot \sigma_{4z}]$	$Q_{21} = \text{CNOT}_{34} \cdot X_4 \cdot \text{CNOT}_{13} \cdot X_3$
$E_{10} = \text{Tr}[\rho_{10} \cdot \sigma_{4z}]$	$Q_{10} = \text{CNOT}_{34} \cdot X_4 \cdot \text{CNOT}_{23} \cdot X_3 \cdot \text{CNOT}_{12} \cdot \bar{Y}_2 \cdot \bar{Y}_1$	$E_{22} = \text{Tr}[\rho_{22} \cdot \sigma_{4z}]$	$Q_{22} = \text{CNOT}_{24} \cdot \text{CNOT}_{12} \cdot X_2 \cdot X_1$
$E_{11} = \text{Tr}[\rho_{11} \cdot \sigma_{4z}]$	$Q_{11} = \text{CNOT}_{34} \cdot X_4 \cdot \text{CNOT}_{23} \cdot \bar{Y}_3 \cdot \text{CNOT}_{12} \cdot X_2 \cdot \bar{Y}_1$	$E_{23} = \text{Tr}[\rho_{23} \cdot \sigma_{3z}]$	$Q_{23} = \text{CNOT}_{23} \cdot \text{CNOT}_{12} \cdot X_2 \cdot X_1$
$E_{12} = \text{Tr}[\rho_{12} \cdot \sigma_{4z}]$	$Q_{12} = \text{CNOT}_{34} \cdot \bar{Y}_4 \cdot \text{CNOT}_{23} \cdot X_3 \cdot \text{CNOT}_{12} \cdot X_2 \cdot \bar{Y}_1$		

sequence, 70% of entanglement is preserved, while with the UR8DD+PR sequence, 82.1% of the entanglement is preserved, whereas the UR8DD+CPR sequence is able to preserve 81.4% of the entanglement. Similarly, for the four-qubit cluster state, the entanglement dies at $1.68\mu s$, and on protecting the state with UR8DD sequence, 54.8% of entanglement is preserved, while with UR8DD+PR sequence, 65.5% of the entanglement is preserved, whereas the UR8DD+CPR sequence is able to preserve 62.6% of the entanglement.

IV. CONCLUSIONS

We have experimentally demonstrated the efficacy of the URDD sequence in preserving multipartite entangled states generated on the IBM quantum computer using superconducting qubits. Our results show that the UR8DD sequence is able to successfully protect the entanglement present in such entangled states. The entanglement witness was utilized to quantify the entanglement present in the state at several time points, and to directly measure

the entanglement present via measurement on only a single qubit. Further, we show that the performance of the basis UR8DD sequence can be substantially improved by adding the PR and CPR variants.

Our work is a step forward in demonstrating the utility of URDD sequences in protecting multipartite entanglement on NISQ computers. Future applications of this work include integrating the URDD sequence with multiqubit quantum gates during free evolution, for gate optimization and protection [53, 54].

ACKNOWLEDGMENTS

Authors acknowledge the support from IBM quantum experience team for providing the experimental platform. Arvind acknowledges financial support from DST/ICPS/QuST/Theme-1/2019/General Project number Q-68. K. D. acknowledges financial support from DST/ICPS/QuST/Theme-2/2019/General Project number Q-74.

-
- [1] M. A. Nielsen and I. L. Chuang, Quantum computation and quantum information (Cambridge university press, 2010).
- [2] E. Schrodinger, Math. Proc. Camb. Philos. Soc. **31**, 555 (1935).
- [3] M. Hillery, V. Bužek, and A. Berthiaume, Phys. Rev. A **59**, 1829 (1999).
- [4] D. Gottesman, Phys. Rev. A **61**, 042311 (2000).
- [5] C. H. Bennett and G. Brassard, Theor. Comput. Sci. **560**, 7 (2014).
- [6] C. H. Bennett, G. Brassard, C. Crépeau, R. Jozsa, A. Peres, and W. K. Wootters, Phys. Rev. Lett. **70**, 1895 (1993).
- [7] C. H. Bennett and S. J. Wiesner, Phys. Rev. Lett. **69**, 2881 (1992).
- [8] T. Yu and J. H. Eberly, Phys. Rev. Lett. **93**, 140404 (2004).
- [9] W. Dür and H.-J. Briegel, Phys. Rev. Lett. **92**, 180403 (2004).
- [10] P. W. Shor, Phys. Rev. A **52**, R2493 (1995).
- [11] A. M. Steane, Phys. Rev. Lett. **77**, 793 (1996).
- [12] E. Knill and R. Laflamme, Phys. Rev. A **55**, 900 (1997).
- [13] L.-M. Duan and G.-C. Guo, Phys. Rev. Lett. **79**, 1953 (1997).
- [14] D. A. Lidar, I. L. Chuang, and K. B. Whaley, Phys. Rev. Lett. **81**, 2594 (1998).
- [15] L. Viola, E. Knill, and S. Lloyd, Phys. Rev. Lett. **82**, 2417 (1999).
- [16] L. Viola, S. Lloyd, and E. Knill, Phys. Rev. Lett. **83**, 4888 (1999).
- [17] K. Khodjasteh and D. A. Lidar, Phys. Rev. Lett. **95**, 180501 (2005).

- [18] L. Viola and E. Knill, Phys. Rev. Lett. **94**, 060502 (2005).
- [19] K. Khodjasteh and D. A. Lidar, Phys. Rev. A **75**, 062310 (2007).
- [20] W. Yang and R.-B. Liu, Phys. Rev. Lett. **101**, 180403 (2008).
- [21] G. S. Uhrig, Phys. Rev. Lett. **102**, 120502 (2009).
- [22] L. P. Pryadko and G. Quiroz, Phys. Rev. A **80**, 042317 (2009).
- [23] J. Du, X. Rong, N. Zhao, Y. Wang, J. Yang, and R. B. Liu, Nature **461**, 1265 (2009).
- [24] Y. Wang, X. Rong, P. Feng, W. Xu, B. Chong, J.-H. Su, J. Gong, and J. Du, Phys. Rev. Lett. **106**, 040501 (2011).
- [25] C. A. Ryan, J. S. Hodges, and D. G. Cory, Phys. Rev. Lett. **105**, 200402 (2010).
- [26] E. L. Hahn, Phys. Rev. **80**, 580 (1950).
- [27] G. S. Uhrig, Phys. Rev. Lett. **98**, 100504 (2007).
- [28] W. Yang and R.-B. Liu, Phys. Rev. Lett. **101**, 180403 (2008).
- [29] M. J. Biercuk, H. Uys, A. P. VanDevender, N. Shiga, W. M. Itano, and J. J. Bollinger, Phys. Rev. A **79**, 062324 (2009).
- [30] S. S. Roy, T. S. Mahesh, and G. S. Agarwal, Phys. Rev. A **83**, 062326 (2011).
- [31] M. Heinze and R. König, Phys. Rev. Lett. **123**, 010501 (2019).
- [32] W. M. Witzel and S. Das Sarma, Phys. Rev. B **76**, 241303 (2007).
- [33] G. A. Álvarez, A. M. Souza, and D. Suter, Phys. Rev. A **85**, 052324 (2012).
- [34] A. M. Souza, G. A. Álvarez, and D. Suter, Phys. Rev. Lett. **106**, 240501 (2011).
- [35] G. T. Genov, D. Schraft, N. V. Vitanov, and T. Halfmann, Phys. Rev. Lett. **118**, 133202 (2017).
- [36] A. M. Souza, Quant. Inf. Proc. **20**, 237 (2021).
- [37] Z.-Y. Wang, J. E. Lang, S. Schmitt, J. Lang, J. Casanova, L. McGuinness, T. S. Monteiro, F. Jelezko, and M. B. Plenio, Phys. Rev. Lett. **122**, 200403 (2019).
- [38] Z. Wang, J. Casanova, and M. B. Plenio, Symmetry **12**, 10.3390/sym12050730 (2020).
- [39] R. Harper and S. T. Flammia, Phys. Rev. Lett. **122**, 080504 (2019).
- [40] M. Sisodia, A. Shukla, and A. Pathak, Phys. Lett. A **381**, 3860 (2017).
- [41] Y. Lee, J. Joo, and S. Lee, Sci. Rep. **9**, 4778 (2019).
- [42] G. García-Pérez, M. A. C. Rossi, and S. Maniscalco, Npj Quantum Inf. **6**, 1 (2020).
- [43] B. Pokharel, N. Anand, B. Fortman, and D. A. Lidar, Phys. Rev. Lett. **121**, 220502 (2018).
- [44] S. J. Devitt, Phys. Rev. A **94**, 032329 (2016).
- [45] M. Horodecki, P. Horodecki, and R. Horodecki, Phys. Lett. A **223**, 1 (1996).
- [46] O. Gühne and G. Tóth, Phys. Rep. **474**, 1 (2009).
- [47] O. Gühne and N. Lütkenhaus, Phys. Rev. Lett. **96**, 170502 (2006).
- [48] C.-J. Zhang, Y.-S. Zhang, S. Zhang, and G.-C. Guo, Phys. Rev. A **76**, 012334 (2007).
- [49] M. Bourennane, M. Eibl, C. Kurtsiefer, S. Gaertner, H. Weinfurter, O. Gühne, P. Hyllus, D. Bruß, M. Lewenstein, and A. Sanpera, Phys. Rev. Lett. **92**, 087902 (2004).
- [50] J. Sperling and W. Vogel, Phys. Rev. Lett. **111**, 110503 (2013).
- [51] O. Gühne and P. Hyllus, Int. J. Theor. Phys. **42**, 1001 (2003).
- [52] Y. Tokunaga, T. Yamamoto, M. Koashi, and N. Imoto, Phys. Rev. A **74**, 020301 (2006).
- [53] A. M. Souza, G. A. Álvarez, and D. Suter, Phys. Rev. A **86**, 050301 (2012).
- [54] J. Zhang, A. M. Souza, F. D. Brandao, and D. Suter, Phys. Rev. Lett. **112**, 050502 (2014).